Propagation characteristics of ultrasonic weld-guided waves in Friction stir welding joint of same material

Yishou Wang[a], Tian Gao[a], Debo Liu[b], Hu Sun[a], Bingrong Miao[c,*], Xinlin Qing[a,*]

[a] *School of Aerospace Engineering, Xiamen University, Xiamen 361005, China*
[b] *Beijing Institute of Astronautical Systems Engineering, Beijing 100076, China*
[c] *State-key Laboratory of Traction Power, Southwest Jiaotong University, Chengdu 610031, China*

ARTICLE INFO

ABSTRACT

Friction stir welding (FSW) is an important technology for manufacturing large-scale aluminum alloy propellant tank. Due to stress corrosion and cyclic loads, the key FSW joints require online monitoring to ensure the structural integrity and service safety of long-term storage propellant tanks. FSW joints in the propellant tank are regarded as a type of circumferential or longitudinal long and narrow region. In order to detect the flaws with high efficiency and fewer sensors, the propagation characteristics of ultrasonic guided waves in the FSW joint of same material is investigated in this paper. The weld of a FSW joint is characterized by concave cross-sectional shape and different microstructure-mechanical parameters. The micro-structure, micro-hardness, and Young's modulus of a real FSW joint are analyzed, and a two-dimensional semi-analytical finite-element (SAFE) method is employed to study the effects of different parameters on the modal characteristics of weld-guided waves in the FSW joint. In the studied fundamental modes (symmetric (S0), anti-symmetric (A0), and shear-horizontal (SH0)), an almost non-leaky A0-like weld-guided wave at a certain frequency range from 100 kHz to 210 kHz is discovered in the welded zone of a specific FSW model and shows a potential for long-distance detection. Parametric simulation results show that A0-like, SH0-like and S0-like modes at 120 kHz always exist when the weld width is changed while the moduli of the welded zone and base metal zone are maintained the same. Additionally, the simulations demonstrate that some weld-guided waves only exist if the modulus value of the welded zone is lower than that of the base metal zone when the cross section is geometrically continuous (i.e. the shoulder plunge depth is zero). Comparing with weld-guided waves affected by weld width, the weld-guided waves affected by the modulus change shows less obvious energy leakage during propagation. The experiments are conducted to validate the existence of A0-like weld-guided mode with a primary energy trapping effect.

1. Introduction

Friction stir welding (FSW), as a new important solid phase welding technology [1–3], has been widely applied in manufacturing mechanical joints of industrial equipment in aerospace, railway, automobile and maritime fields. For example, the FSW technology is used to manufacture large-scale thin-walled aluminum alloy propellant tanks and high-speed bogie frames in order to reduce production costs and shorten delivery time. Although FSW has significant advantages (e.g. low residual stress, high mechanical properties and environment-friendly process) [2], FSW joints of components or parts are a matter of concern when they are working in a complex dynamic environment. Taking long-term storage metal propellant tanks for example, the propellant tanks are often in different states such as storage, transport and duty due to different mission requirements [4]. They often bear many kinds of loads for a long time, such as internal pressure, vibration, temperature, impact and stress corrosion. These complex loads may cause the performance degradation and defect growth of FSW joints.

Generally, the FSW parts and components before their operation are required to be carefully checked by nondestructive detection methods such as X-ray method [5], ultrasonic methods [6] and eddy current method [7,8]. However, some internal microdefects (e.g. weak connections and worm holes) generated in the welding process may fail to be detected due to the limitation of instruments. These defects will further grow up and induce new microcracks around high stress concentration region due to the comprehensive effects of various loads in service, and corrosion pits are easy to appear near the weld during long-term storage and service. Therefore, it is necessary to monitor the FSW joints in real time in order to ensure the structural integrity and service safety of long-term storage propellant tank.

Ultrasonic guided waves (GWs, in a plate called as Lamb waves) methods have shown great potential in aerospace applications to detect and monitor damages in plate-like metal or composite structures, since GWs are sensitive to defects such as cracks, corrosion, and delamination [9–14]. Guided waves can travel over long distances and have high detection efficiency in a way of area scanning. Making use of traditional guided waves is required to permanently attach many PZT sensors in order to identify small damages or flaws in large-area structures. However, the weld features generated by FSW and fusion welding have not been of special concern. Until recently, feature guided waves (FGW) regarded as one particular branch of GWs are getting more and more interest and attention [15–18], because FGW modes can propagate long distances and quickly inspect the flaws of long-range features where the wave energy is strongly confined. Several important research teams directed by Prof. Fan, Prof. Castaings and Prof. Lowe have made very valuable theoretical and experimental works on FGW in welded metal plates and composite plates with complex shapes such as bends, spars, stiffeners and ribs [16,19–26]. The modal and dispersion characteristics of FGW are often analyzed by two-dimensional semi-analytical finite element (SAFE) and 3D finite element simulation. The FGW signals are acquired by Laser interferometer [26] and fiber bragg grating sensors [27]. FSW joints in a propellant tank can be regarded as circumferential or longitudinal long and narrow regions. It is natural to ask whether the guided waves can propagate in this region along the weld direction to form weld-guided waves. If the answer is yes, the FGW modes can be used to detect the flaws in a way of much higher efficiency and less sensors. This is the initial motivation of the current study.

There are several studies on the propagation behaviors of ultrasonic guided waves in the FSW plate of similar and dissimilar materials [28–31]. From the viewpoint of reflection and transmission, Fakih et al. [30,32] investigated the numerical and experimental propagation behavior of the fundamental Lamb-wave modes upon interaction with welded joints of dissimilar materials by changing incidence angles normal to material interface. Tarraf et al. [29] focused on the characterization of guided waves behavior in similar and dissimilar materials FSW plates through an often used sensor network. Through comparing the amplitude and reflection of signals in the path across the welded zone of FSW plate, they obtained two interesting findings that no additional considerations are required for applying weld-guided waves in similar-materials FSW plates and the weld line within dissimilar-material welded plate showed the material discontinuity results in guided wave scattering. However, the propagation behavior of guided waves in the FSW joint along the weld direction was not further investigated, as well as the difference between the feature guided waves and the traditional guided waves in terms of dispersion and attenuation. Meanwhile, no studies focusing on the effect of the cross-sectional shape of FSW joints on FGWs were founded in the literature. Predoi et al. [24] have investigated the presence of specific and original guided modes in a grooved aluminum plate, which can provide an useful referential value.

Comparing with studies on FGWs in FSW joints, there are more investigations on the propagation characteristics of guided waves in fusion welded joint. Through the experimental measurement using a single edge-mounted transducer, Sargent [15] firstly proposed the concept of "weld-guided waves" that the similar S_0 mode Lamb wave is easily confined to the weld and propagates along the weld of a butt-welded steel plate made by submerged arc welding. The results showed the weld-guided waves would provide a potential means for corrosion detection in heat affected zone. Juluri et al. [33] observed a significant guiding effect of waves propagating along the butt weld of a plate and exploited the decay rate at different frequencies, which were confirmed by FE simulation on an idealized weld. To further explore the properties of weld-guided waves in a way of systematic analysis, Fan et al. [18,21] conducted very valuable studies on the propagation behavior of S0-like and SH0-like modes in the weld using SAFE method, as well as their interaction with defects in the butt-welded joint. It was found that the

non-leaky and almost non-dispersive SH0 mode FGWs was attractive for long distance inspection. The interesting results such as energy trapping and reflection ratio were validated by 3D FF simulations and experimental measurements. Recently, Yu et al. [20] have made an interesting and systematic work on FGWs in an unbounded fusion welded steel plate by integrating SAFE approach with the perfectly matched layers to obtain the potential higher order modes. They proposed a novel superposition technique to separate the multiple high order SH signals such that the energy trap phenomenon of ultrasonic guided waves in the weld was found by simulation and verified by experiments. According to above work, it can be concluded that the fundamental and higher order SH types weld-guided waves exist in the fusion welded joint and in particular, SH0-like mode is non-leaky and almost non-dispersive.

Although many researches on the propagation behavior of weld-guided waves focusing on the fusion welding joints have been conducted, few researches are focusing on same-material FSW joints. Therefore, it is necessary to conduct parametric studies on the propagation characteristics of weld-guided waves in the same-material FSW joint in order to reveal the effect of the geometric discontinuity and the differences in mechanical parameters on the propagation behavior of FGWs. In this paper, two kinds of factors in terms of cross-sectional geometric shape and microstructure-mechanical properties are analyzed to reveal their effects on the propagation behaviors of weld-guided waves in Section 2, Based on the measured mechanical parameters of a real FSW joint, a FSW model is built to study the characteristics of guided waves in the FSW joint using SAFE method in Section 3. In the following section 4, respective parametric study involved with the concave cross-sectional shape and elasticity modulus is performed at a single frequency. In Section 5, the validation experiments were conducted to illustrate an energy trapping effect in the weld region when A0-like weld-guided waves propagate along weld direction. Last section made a conclusion for the paper.

2. Analysis of factors affecting weld-guided waves in the FSW joint

It is well known that the structural feature variations will affect the propagation behaviors of guided waves [24]. It has been validated that the non-leaky SH0 and high order SH modal weld guided waves exist in the fusion weld joint with convex cross section [18,20,21]. The cross sectional feature of FSW joint is generally concave. Meanwhile, the microstructure-mechanical properties of the weld and the base metal are different and the interface will be formed, especially for dissimilar material welded joint. Therefore, this section analyzes the possible factors that will affect the propagation behaviors of weld-guided waves. The microstructure-mechanical properties of a real FSW plate are tested to provide data support.

2.1. The weld cross sectional comparison between FSW joint and fusion welded joint

The welding process of FSW technology is briefly described as follows. A high-speed rotating tool composed of a shoulder and a pin moves along the welding direction after it is inserted into the joint area between two work pieces, as shown in Fig. 1. Friction heat generated at the contact area between the stirring head and the work pieces leads to the formation of plastic softening layers near the metal. The softening layers fill the cavity formed behind the stirring pin under the rotating action of the tool. The connection of the materials is realized under the stirring of the pin and the extrusion of the shoulder [34]. FSW is carried out in solid phase at a temperature lower than the melting point of the material, and doesn't require filler material and protective gas. FSW can realize the connection of the same or different materials. Generally, the parts with the same material are connected by FSW to form a complete component like propellant tank, as shown in Fig. 1(b).

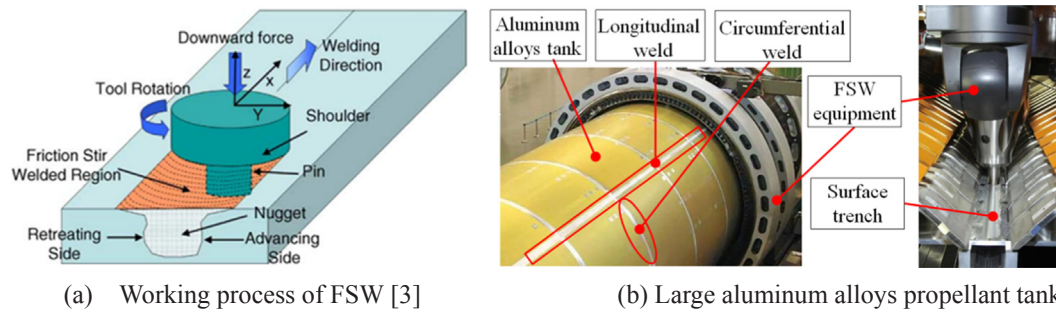As shown in Fig. 1, the surface trench is formed in the top surface of

(a) Working process of FSW [3]

(b) Large aluminum alloys propellant tank

Fig. 1. Schematic diagram and classical product of FSW.

the FSW joint when the tool is moved along the welding line to produce a FSW joint. Generally, the surface trench is unavoidable because the rotating tool is inserted into the top surface of workpieces to be welded until the shoulder is embedded into the workpiece to a certain depth defined as shoulder plunge depth [35]. Therefore, the application of shoulder plunge depth makes the top surface of a FSW joint lower than that of base metal, which inevitably leads to the weld thinning phenomenon in FSW joints [36]. That is to say that the weld cross section is concave on one side. The width and shape of the concavity depends on the diameter and shape of the shoulder.

There are several negative effects of weld thinning, including flash formation, the reduction of the serviceable load and stress concentration. Some researchers have done many work to eliminate the surface trench of a FSW joint, including the improvement of welding tool structure, and additive or subtractive treatment before or after welding [37]. However, for large propellant tanks made by FSW, the additive or subtractive treatment is not applicable to eliminate surface trench. This is the motivation to perform the current parametric study of geometric discontinuity of the weld cross section. For some fusion welding process, the height of welded zone is higher than that of base metal zone, which means that the cross-sectional feature of the welded zone is a convex arc shape in geometry. The cross-sectional comparison of the welded zones between FSW joints and fusion welded joints are illustrated in Fig. 2. Generally, the cross section of butted welded joint is convex on both sides due to the welding process, as shown in the literature [18,20].

2.2. Analysis of microstructure-mechanical characteristics of the FSW joint

Generally, the microstructure-property characteristics of a FSW joint are seriously affected by different combination of process parameters such as the ratio of rotational speed to welding speed, the tool geometry and the plunge depth. From the aspect of microstructure, a FSW part is divided into base metal zone (BMZ), heat affected zone (HAZ), thermo-mechanically affected zone (TMAZ) and nugget zone (NZ) [38], as shown in Fig. 3. The welded zone (WZ) consists of TMAZ and NZ. It is well known that the grains in the weld of FSW part will be refined [39]. As shown in Fig. 3(b), there are three interfaces among NZ, TMAZ, HAZ and BMZ. For the similar and dissimilar material FSW

plate, a material interface between WZ and BMZ can be formed, where the material discontinuity occurs [30]. More generally, the material discontinuity also exists in the same material FSW plate due to different microstructure-mechanical characteristics of four zones. The existing results have shown that the ratio of the average grain diameter of BMZ to that of WZ is up to 10 for the 6061-T6 aluminum FSW plate [38], while the Vickers hardness of WZ is higher than that of BMZ. Therefore, it is worth considering that whether these differences of microstructure-mechanical characteristics in the welded zone and BMZ affect the propagation of guided waves in the FSW joint.

Considering that the 2219 aluminum alloy commonly used as the material of propellant tank structure, two 2219 aluminum alloy FSW specimens were manufactured by Ningbo Youzhi and Aerospace Engineering Equipment Co., Ltd. The 3D dimensions and geometric weld parameters of the FSW specimens are listed in Table 1, where the specimen length is along weld direction. Other FSW process parameters are unknown due to business reasons. These FSW specimens are perfectly welded without internal flaws. To obtain the detailed information of microstructure-mechanical properties of the FSW joint, three small test specimens are cut from Specimen I by the electric spark numerical control cutting machine. The information on size and location of three test specimens is shown in Fig. 4. The transverse sections of three small specimens S1, S2 and S3 were used to analyze the properties of WZ, HAZ and BMZ, respectively. Before measurement, three specimens were processed by test standards such as coarse and fine grinding, diamond polishing solution and surface etch with Keller reagent.

The microstructure-mechanical properties of three specimens included the metallographic structure, the microhardness, the Young's modulus and the material density. The metallographic structures were observed by the ZEISS Axio Observer 3 m metallographic microscope. The microhardness was measured by INNOVA TEST FALCON 500 microhardness tester. The Young's moduli were measured by Anton Paar NHT3 nanoindenter. The densities of WZ and BMZ were measured by a METTLER TOLEDO densitometer.

The observed cross-sectional metallographic structures of the three regions are shown in Fig. 5. From Fig. 5 (a), it can be seen that the microstructure of NZ is more uniform and the grains are obviously refined under the strong stirring and friction, compared with the grains in TMAZ affected by stirring and heat. Meanwhile, there is a clear
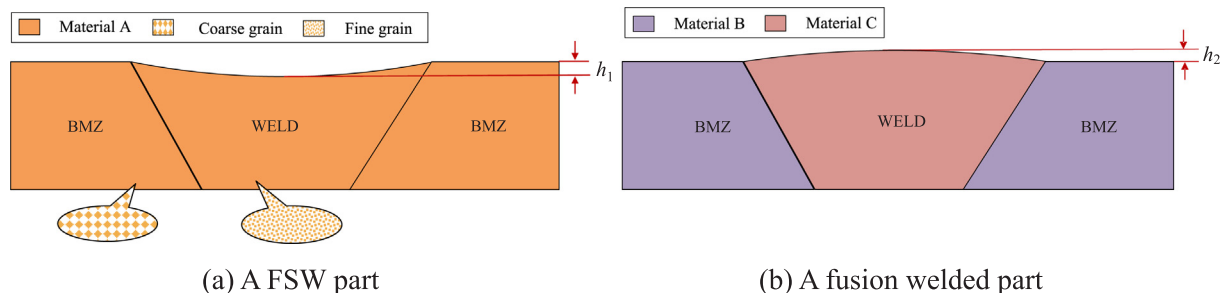

(a) A FSW part

(b) A fusion welded part

Fig. 2. Comparison between fusion welded part and FSW part.

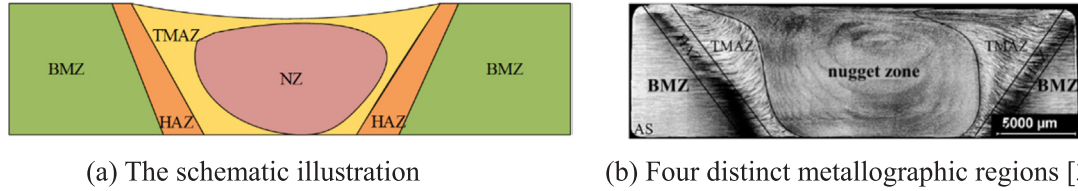(a) The schematic illustration   (b) Four distinct metallographic regions [34]

Fig. 3. Microstructure zone division of FSW part.

Table 1
The dimensional information of two types of 2219 aluminum alloy FSW plates.

ID	Length	Width	Thickness	Weld width	Plunge depth (h_1)
I	320 mm	300 mm	7 mm	20 mm	1 mm
II	1050 mm	300 mm	6 mm	18 mm	1 mm

boundary line or interface marked by a red dotted line between TMAZ and NZ, which is similar with that of Fig. 2(b). The microstructure and grains of HAZ only affected by heat are almost the same with those of BMZ, as shown in Fig. 5(b) and (c). The reason for unobservable interface between TMAZ and HAZ is that this interface region is very small as shown in Fig. 2(b), which maybe had been destroyed when these three test specimens were cut from a whole specimen. It will be better to perform the metallographic analysis on a whole weld cross section, which is limited by the current available instrument. In summary, there is a significant difference in the microstructure between WZ and BMZ. It should be noted that the minimum wavelength (about 6.7 mm) of ultrasonic guided waves at a given frequency range from 100 kHz to 500 kHz is far greater than the microstructure size (0.5 mm × 0.4 mm in length and width estimated by 100 μm scale) and the welded zone and heat affected zone can be approximately regarded as isotropic homogeneous medium.

As shown in the two right figures of Fig. 4, the fifteen evenly spaced points on the section of S1 specimen are used to measure the microhardness of the welded zone, while the eleven evenly spaced points on the section of S2 and S3 for the microhardness testing of HAZ and BMZ, respectively. In the process, the 0.98 N load perpendicular to the test surface was applied to these test points with 10 s holding time in sequence from left to right. The measurement data of three specimens was shown by solid blue dots and plotted by a fitting curve, as shown in Fig. 6. It can be clearly seen that the microhardness of WZ and BMZ were significantly different. As a transition zone, the microhardness of HAZ was gradually increased along the direction from HAZ to BMZ.

According to above measured results, there was no obviously observable interface between HAZ and BMZ or WZ. It was difficult to distinguish HAZ in the experimental FSW joint. Therefore, only WZ and BMZ were analyzed in the Young's modulus and density measurement experiments. Three rows of points (totally 45 points) were tested on the region of S1 and S3 respectively, as shown in Fig. 4. Each specimen was repeatedly measured six times to eliminate the gross error and the average value was taken as the final density measurement result. The

measurement results of Young's modulus (E) and the density (ρ) in the welded zone and the base metal zone are shown in Table 2. It can be seen that the density of WZ is almost the same with that of BMZ and their relative error is very small (0.43%). It can be demonstrated that there is an obvious difference in Young's modulus between WZ and BMZ. These measured material parameters were also used in the following finite element analysis, where the density of WZ and BMZ is viewed as the same (ρ = 2820 kg/m^3).

In summary, due to complex thermal-mechanical coupling effects, there are significant differences in the microstructure and mechanical properties between the welded zone and the base metal zone of the same material FSW part. This microstructure discontinuity is possible to affect the propagation characteristics of weld-guided waves.

3. Simulation of weld-guided waves by SAFE method

The semi-analytical finite-element (SAFE) method has gotten more and more attentions for the propagation characteristics study of waveguides with irregular cross section and anisotropic material [23,24]. The advantage of SAFE method is the reduction of the computational cost by converting the three-dimensional elasticity model into the two-dimensional model. It is much easier to obtain the dispersion curve and carry out parametric analysis. To identify and understand feature-guided waves existing in a FSW joint, simulation is performed by using SAFE method to represent the cross section of the waveguide and a description along the propagation direction.

3.1. The theory of SAFE

The theory of SAFE in solids is based on the three-dimensional linear elastic solid mechanics. Two parameters (e.g. material density and elastic constants) are introduced into the equation of displacement in order that the model can fit to tackle with irregular cross section and anisotropic material. As show in Fig. 7, for a given mass point in the cross section of a FSW plate, the equation of dynamic equilibrium can be described in Eq. (1) [20].

$$\sum_{j,k,l=1}^{3} \left[C_{ikjl} \frac{\partial^2 U_j}{\partial x_k x_l} \right] + \rho \omega^2 U_i = 0; \quad i = 1, 2, 3. \tag{1}$$

where C_{ikjl} are the stiffness moduli, being real or complex values for elastic and viscoelastic materials respectively, U is the displacement vector, ρ is the mass density, $\omega = 2\pi f$ is the angular frequency, f is the
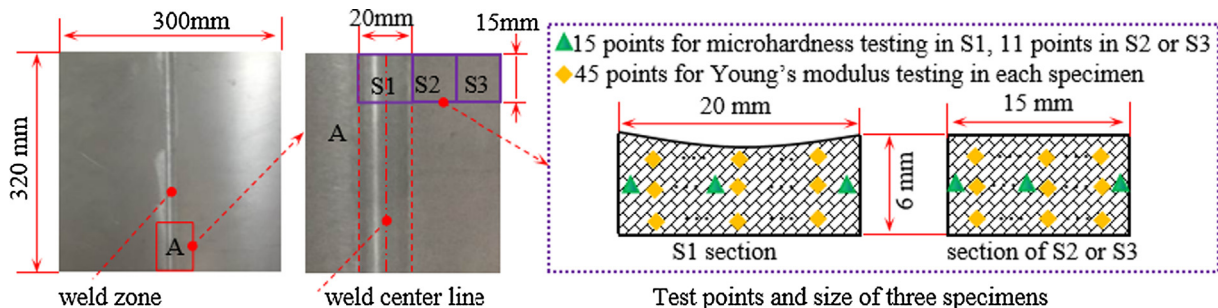

Fig. 4. The schematic illustration of three test pieces cut from Specimen I.
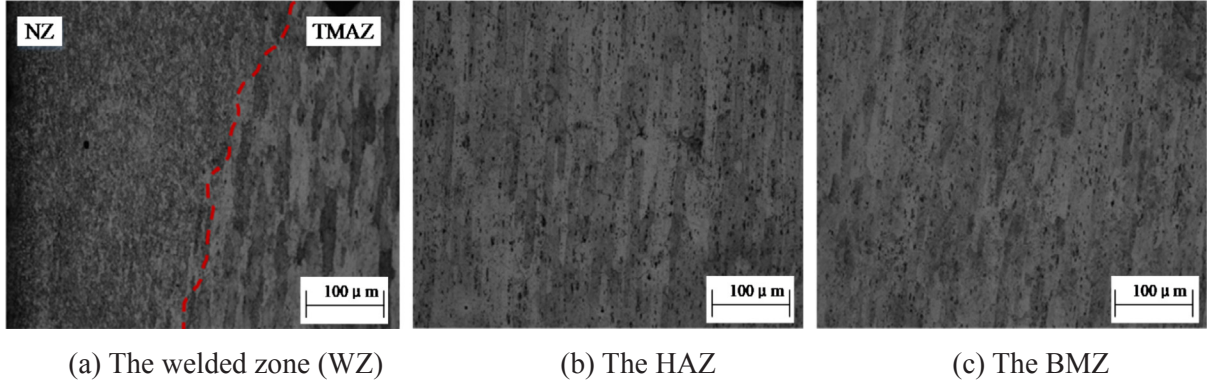
(a) The welded zone (WZ)   (b) The HAZ   (c) The BMZ

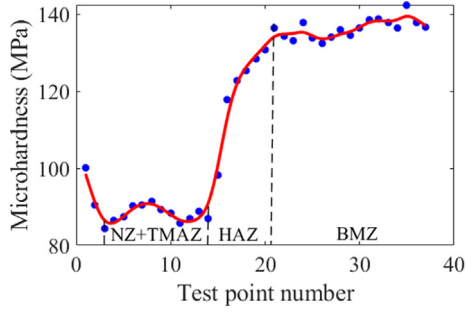**Fig. 5.** Metallographic images of microstructure of a FSW specimen.

Fig. 6. The microhardness data of test points and their fitting curve.

Table 2
The measured material parameters.

	The welded zone	The base metal zone
E(GPa)	85.34	79.69
ρ(kg/m^3)	2832	2820

frequency, and the subscript $i = 1,2,3$ indicates coordinate index. The stresses on the boundaries of a given domain are written as (2):

$$T_i = \sum_{j,k,l=1}^{3} C_{ikjl} \frac{\partial U_j}{\partial x_l} n_k \tag{2}$$

where n_k is the component of **n**, the outward unit vector normal to the boundary of the domain.

Suppose that the harmonic guided waves propagate along the Ox_3 axis (Fig. 7), then the displacements vector in the wave-guide can be represented by the formula (3).

$$u_i(x_1, x_2, x_3, t) = U_i(x_1, x_2)e^{I(Kx_3 - \omega t)}; I = \sqrt{-1} \tag{3}$$

where K is the wavenumber along the direction Ox_3 and t is the time variable, and the subscript $i = 1, 2, 3$.

Substitute the Eq. (3) into the Eq. (1) and the Eq. (2), respectively, these two equations can be rewritten as Eqs. (4) and (5) in a form of an eigenvalue problem.

$$C_{ikjl} \frac{\partial^2 U_j}{\partial x_k \partial x_l} + I(C_{i3jk} + C_{ikj3})\frac{\partial(KU_j)}{\partial x_k} - KC_{i3j3}(KU_j) + \rho\omega^2\delta_{ij}U_j = 0 \tag{4}$$

$$T_i = C_{ikjl}\frac{\partial U_j}{\partial x_l}n_k + IC_{ikj3}(KU_j)n_k \tag{5}$$

where the indices $j = 1, 2, 3$ and $k, l = 1, 2$. In the commercial FE model (COMSOL), the partial differential equations of matrix coefficients and Neumann boundary conditions are used to obtain the eigenvalue (i.e. wavenumber) and eigenvector (i.e. vibration modes) at a chosen frequency.

$$\nabla\cdot(c\nabla\widetilde{U} + \alpha\widetilde{U} - \gamma) - \beta\nabla\widetilde{U} - a\widetilde{U} + \lambda d_a\widetilde{U} - \lambda^2 e_a\widetilde{U} = 0 \tag{6}$$

$$\mathbf{n}\cdot(c\nabla\widetilde{U} + \alpha\widetilde{U}) + q\widetilde{U} = 0 \tag{7}$$

where all matrix coefficients admit complex values, which is essential for viscoelastic materials, $\widetilde{U}$ represents the set of variables to be determined. Full implementation details for this method were given by Predoi et al. [24].

The detailed statement of SAFE theory can be found in the literature [20,23,24]. In summary, the nature of SAFE method is to seek eigenvalues of wavenumber K for different given angular frequency ω, then calculate the axial component of the energy flow in the wave propagation Ox_3 and the three-dimensional displacement (i.e. modal shapes) at each nodal position of the mesh for each eigenvalue solution that makes sense. The energy flow and the displacement in the axial direction are used to judge whether the weld-guided waves exist or not as well as the corresponding wave modes. Finally, the velocities of given wave mode are calculated under a certain frequency range to obtain its
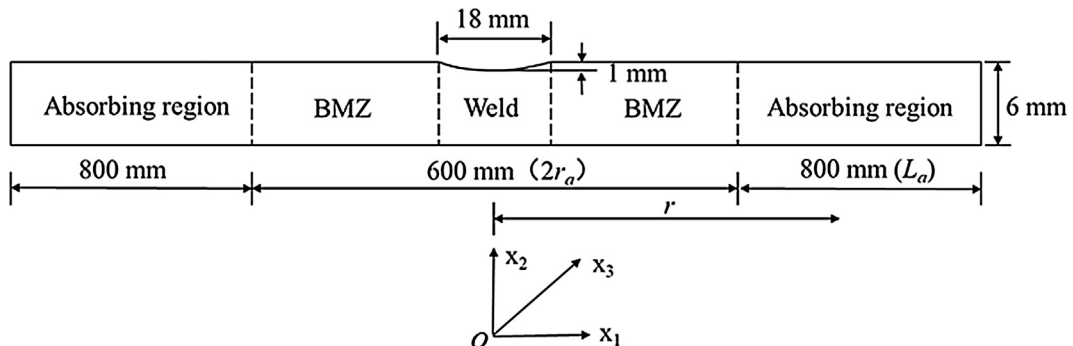

Fig. 7. The schematic of the two-dimensional SAFE model of a FSW plate.

dispersion curves.

3.2. Simulation model of SAFE

According to the actual size of the type II specimen in Table 1 and the measured material parameters in Table 2, the SAFE model of the given FSW plate is developed in the commercial software COMSOL. The information of model sizes and the coordinate system are shown in Fig. 7. The whole geometry is meshed by free triangular elements that are automatically generated by the software. The total number of degrees of freedom is 36246. Continuity of displacements and stresses is imposed at the interfaces between the BMZ and the absorbing region. Stress-free conditions are applied to the outer boundaries enclosing the whole domain. An 800 mm long absorbing region has been added at each side of the plate to avoid reflections from the edge. This absorbing region has the same mass density and elastic properties as BMZ. Based on the work of Castaings et al. [23], the 800 mm length is twice the maximum wavelength of any radiated wave in the studied frequency range (100 kHz–500 kHz). The viscoelasticity of absorbing region gradually increases with the distance away from the central axis of the system by gradually increasing the imaginary parts of its elastic moduli expressed in Eq. (8).

$$C_{ija} = C'_{ij}\left[1 + I\alpha_1\left(\frac{|r-r_a|}{L_a}\right)^3\right] + IC''_{IJ}, \ I = \sqrt{-1} \tag{8}$$

where C'_{ij} is the stiffness of the BMZ plate, C''_{ij} its viscoelasticity; a_1 is a proportion coefficient of the viscoelasticity at the outer limit of the absorbing region, r_a is the distance between the inner border of the absorbing region and the central axis, L_a is the length of the absorbing region, r is the position in the absorbing region with respect to the weld central axis in the $x1$ direction., C_{ija} are the resulting viscoelastic moduli of the absorbing region.

3.3. Weld-guided waves

The eigenvalues (i.e., wavenumber K) and their corresponding eigenvector (i.e., wave mode) are solved successively in the frequency range from 100 kHz to 500 kHz with a step of 10 kHz. The axial component P_{x3} of energy flow at each node position for each corresponding eigenvalue are calculated in order to observe the energy flow distribution in the whole cross section and determine the possible modes of weld-guided waves. The quantity P_{x3} is expressed by the following formula (9) [20].

$$P_{x3} = -\text{Re}\left[\left(\frac{I\omega}{2}\right)(u_1^*\sigma_{31} + u_2^*\sigma_{32} + u_3^*\sigma_{33})\right] \tag{9}$$

where σ_{31}, σ_{32} and σ_{33} are the axial stress components and u_1^*, u_2^* and u_3^* are the complex conjugate of the horizontal, vertical and axial displacements, respectively.

This study just focuses on fundamental modes (symmetric (S0), antisymmetric (A0), and shear-horizontal (SH0)), namely, the eigenvalues near the wavenumber of A0, SH0 and S0 mode guided wave are searched for in the frequency range from 100 kHz to 500 kHz. According to calculation results, only A0-like weld-guided waves in a frequency range from 100 kHz to 210 kHz are found in the weld zone of a given FSW plate. As shown in Fig. 8, the modal properties of A0-like weld-guided waves at a frequency of 120 kHz are illustrated in terms of the energy flow distribution, the axial power flow and the displacement mode shape.

From the Fig. 8(a), it can be seen that a snapshot of the axial component of energy flow means the energy of A0-like mode weld-guided waves is mainly concentrated in and around the weld with little leakage. From Fig. 8(b), it is also found that the mode guided along the weld is dominated by vertical displacement u_2 with respect to the horizontal displacement u_1 and axial displacement u_3, which is similar

to an A0 modal wave in a plate. This almost no-leaky A0-like mode is for the first time observed in a FSW joint, and could be of high interesting for long-distance inspection along FSW joints.

When the imaginary part of the stiffness moduli is introduced, the propagation wavenumbers become complex (i.e. $K = k' + Ik''$) for a guided wave mode at a certain frequency. The imaginary parts (k'') represent the attenuation due to the leakage from the weld to side plates, and the attenuation a can be calculated by the Eq. (10).

$$a = 20\log_{10}\left(e^{k'}\right) \tag{10}$$

The imaginary part k'' of the wavenumber of A0-like mode stays zero or very small at the given frequencies from 100 kHz to 210 kHz, which means that A0-like mode is almost no-leaky and the value of a is zero.

3.4. Dispersion curves

The complex wavenumbers of a given mode at different frequencies can be solved using SAFE method. The corresponding phase velocity (C_p) and group velocity (C_g) can be calculated using the real component k' of complex wavenumber, expressed by the Eq. (11).

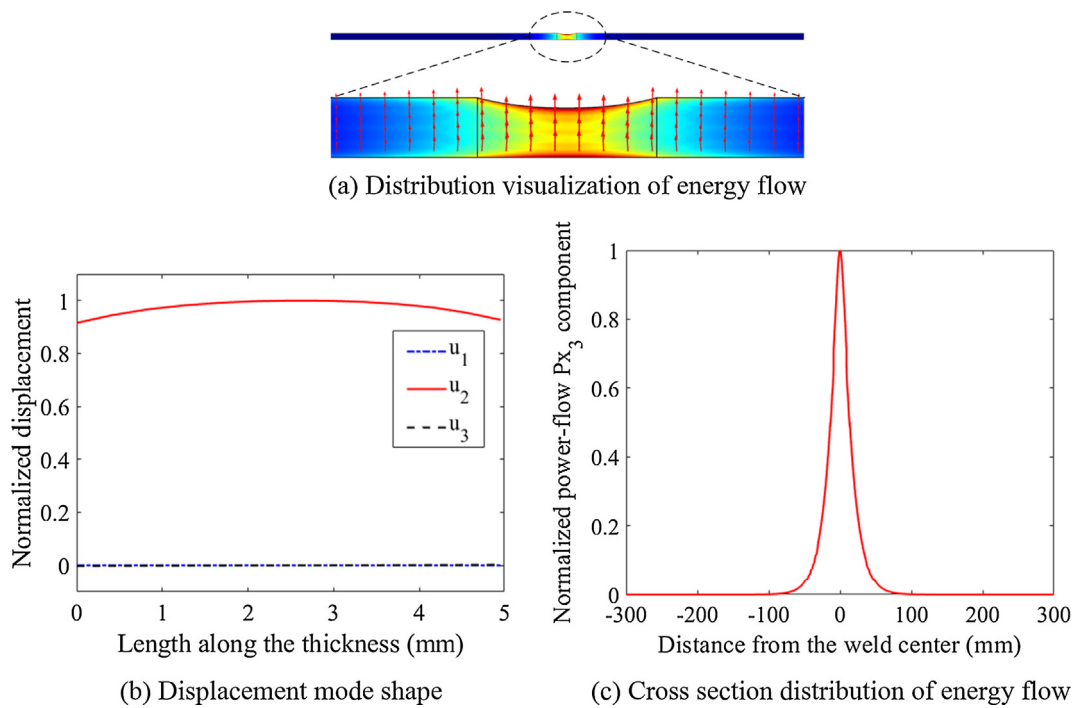$$\begin{cases} C_p = 2\pi f/k' \\ C_g = d\omega/dk' = C_p^2/(C_p - f\cdot(dC_p/df)) \end{cases} \tag{11}$$

The dispersion curves of A0-like weld-guided waves can be obtained by repeating the eigen-calcuations over a given frequency range from 100 kHz to 210 kHz. The dispersion curves of phase velocity and group velocity of A0-like mode are potted in Fig. 9(a) and (b), respectively. The phase velocity and the group velocity of the A0 mode in an aluminum plate are calculated by Dispersion Software. From these figures, it can be seen that A0-like mode in the weld, their dispersion curves of phase velocity and group velocity have the same variation trend with those of corresponding A0 mode in the plate. Meanwhile, it can also be found that the phase velocity of A0-like mode are lower than that of similar modes at a certain frequency range from 100 kHz to 210 kHz, respectively. Therefore, it can be concluded that A0-like mode weld-guided waves can propagate energy only along the weld interface according to the well-known Snell-Descartes law [40]. This law applied weld-guided waves can be stated as follows: if the phase velocity of a given fundamental mode in the weld is smaller than that in the single plate, the energy of the guided waves will be most concentrated in the weld zone with little leakage into the adjacent plate.

4. Parametric analysis of changes in geometric shape and mechanical parameters

According to the numerical results of Section 3, it has been shown that there is only A0-like weld-guided wave in the given FSW model of a real FSW plate, where the cross section is concave shape on a top side, and the elasticity modulus of WZ and BMZ is different. The observation from above simulation is very different from the results obtained in the fusion weld joint [18]. Therefore, it is necessary to conduct a respective parametric study based on the SAFE method to reveal the influence of different factors (i.e. weld width and modulus ratio) on propagation characteristics of weld-guided waves, in this study, called as the width-change weld-guided waves and the modulus ratio-changed weld-guided waves, respectively.

4.1. Declaration of the parameters

As stated in Section 2, the concave geometric shape of a weld cross section depends on two process parameters, i.e., the shoulder diameter and the plunge depth of the shoulder. Generally, these two parameters affect not only the surface quality, but also the microstructures-

(a) Distribution visualization of energy flow

(b) Displacement mode shape

(c) Cross section distribution of energy flow

Fig. 8. The modal properties of weld-guided waves propagating along the weld of FSW plate, derived from the SAFE calculation at 120 kHz. (a)The visualized distribution of energy flow in the cross section (colour coding indicates its relative amplitude (blue: low to red: high)); (b) three displacement components along the thickness and (c) the power-flow P_{x3} component along x_1 direction. (For interpretation of the references to colour in this figure legend, the reader is referred to the web version of this article.)

mechanical characteristics of the weld zone. The shoulders commonly used are characterized by fillet feature, and produce the concave cross section of the welded joint. For a given diameter D of the shoulder, it can be seen that the weld width is determined by the diameter and fillet radius of the shoulder and the plunge depth h_1. In this parametric study, the only variable parameter is the weld width (W), considering that the shoulder plunge depth generally varies in a relatively narrow range for good weld appearance formation, while the plunge depth is fixed as 1 mm. This first parametric study is to investigate the single effect of cross-sectional geometric shape change on the propagation characteristics of guided waves, when the modulus values of different zones are the same for the same material FSW plate.

The parameters about microstructure-mechanical properties of a FSW joint include the grain size, the microhardness, the Young's modulus (E), and the density (ρ). The latter two factors (E and ρ) are required to apply the SAFE method. Considering that the density of WZ and BMZ is almost not changed for the same material FSW joint, this

study selects the ratio of the modulus of BMZ to that of WZ as a control variable (i.e. $r = E_{BMZ} : E_{WZ}$), while the density of two zones is the same, and the shoulder plunge depth is zero. This second parametric study is to investigate the single effect of elastic modulus change on the propagation characteristics of weld-guided waves, when the weld geometry feature is eliminated by a special process or means.

The values of different parameters in the two parametric studies are listed in Table 3. The thickness of the FSW joint, the modulus and density of BMZ in the SAFE model are fixed constant values.

4.2. Parametric analysis of the width-change weld-guided waves

In this parametric analysis, only variable parameter is the weld width, without considering the difference in the modulus and density between WZ and BMZ. As stated in Section 3, there is only A0-like weld-guided wave at a frequency range from 100 kHz to 210 kHz by SAFE method for the highlighted case of Table 3. The parametric studies

(a) Dispersion curves of phase velocity

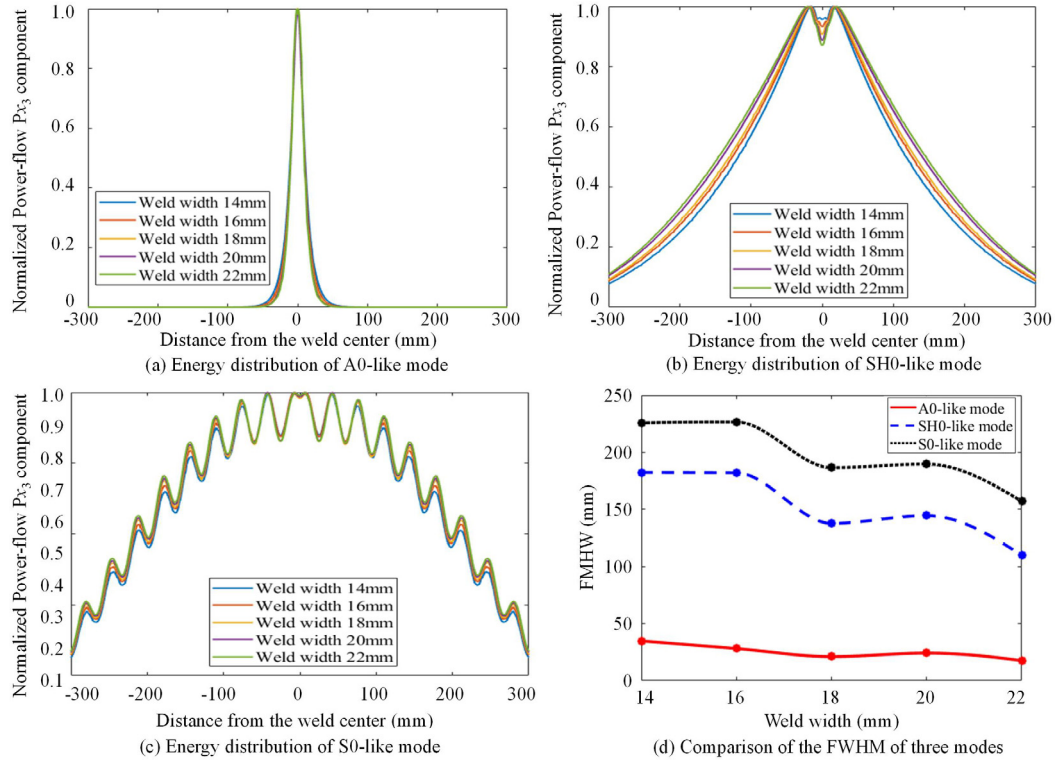(b) Dispersion curves of group velocity
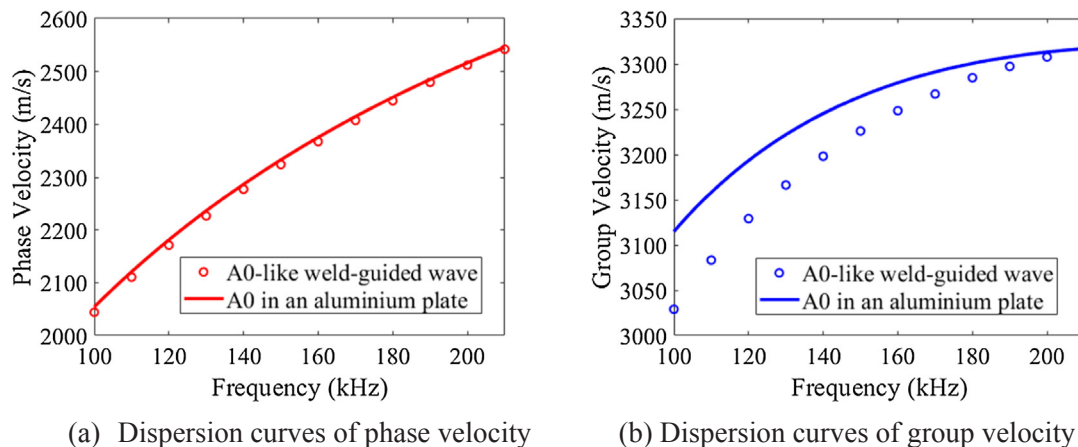
Fig. 9. The dispersion curves of phase and group velocity of A0-like weld-guided waves and A0 mode in the plate.

Table 3
The different values used in a respective parametric study.

Constant parameters			Parametric analysis of W			Parametric analysis of r				
h (mm)	E_{BMZ} (Gpa)	ρ (kg/m³)	W(mm)	h_1(mm)	$r = E_{BMZ} : E_{WZ}$	$r < 1$	$r > 1$	h_1(mm)	W(mm)
6	79.69	2820	14	1	1:1	1:1.3	1:0.9	0	18
			16			1:1.2	1:0.8		
			18			1:1.1	1:0.7		
			20			1:1.07	1:0.6		
			22				1:0.5		

Fig. 10. Normalized power-flow Px_3 component of three modes in different cross sections at 120 kHz.

focus on the three fundamental modes of weld-guided waves in the same frequency range for different weld width. From the calculation of SAFE, A0-like and SH0-like weld-guided waves are found in above frequency range, while S0-like weld-guided waves are found only in the frequency range from 100 kHz to 190 kHz. As for five kinds of cross-sectional weld widths, these weld-guided waves at 120 kHz are illustrated in terms of the axial power flow, as shown in Fig. 10(a)–(c). Meanwhile, the results of A0-like weld-guided waves in parametric studies are very similar to those in Section 3, which means the energy of A0-like mode is easily concentrated in and around the weld when the weld width changes.

The energy distribution of different guided modes in the cross-section across the weld is important to understand their propagation characteristics. This study adopts the concept of full width half maximum (FWHM) [21] to quantitatively compare the energy distribution of three weld guided modes in the cross-section with different widths, as shown in Fig. 10(d). As stated in the literature [21], the smaller the value of the FWHM is, the more energy is concentrating in and around the weld zone. It can be confirmed that the energy of A0-like weld guided mode is more easily concentrated in and around the weld than those of S0-like mode and SH0-like mode.

Meanwhile, three weld-guided waves at 120 kHz are described in terms of the energy flow distribution and the displacement mode shape, as shown in Fig. 11. As for SH0-like mode, it is found that both the

energy flow and the axial component gradually decay with distance away from the weld center, which means the energy of SH0-like mode will partially leak into the BMZ plate. From the Fig. 11(b1), it is also illustrated that the mode guided along the weld is dominated by horizontal displacement u_1 with respect to the vertical displacement u_2 and axial displacement u_3, which is similar to a SH0 wave in a plate. It would be interesting to compare the current SH0-like mode in the FSW joint with SH0-like mode in the fusion weld joint in the literature [18]. Different cross-sectional geometric shapes (concave or convex) will affect the energy leakage of SH0-like weld-guided waves, as shown in Fig. 10(b).

As for S0-like mode, it is shown that both the energy flow and the axial component zigzag change with distance away from the weld center, which indicates the dramatic leakage of the S0-like mode energy will take place and the leaky wave will be radiated at an angle θ_{leak} defined in the literature [18,23]. From the Fig. 11(c2), it is found that the axial displacement u_3 dominates the weld-guided mode in the center of the plate along Ox_1, which is similar to a S0 wave in a plate. This observation is similar with that in the fusion weld joint [18].

In a sum, there exists almost non-leaky A0-like mode, leaky SH0-like and S0-like fundamental modes at a certain frequency range from 100 kHz to 190 kHz in the welded zone when only the geometric feature of the weld cross section is changed. These weld-guided waves are called as width-change dominated weld-guided waves. Meanwhile,
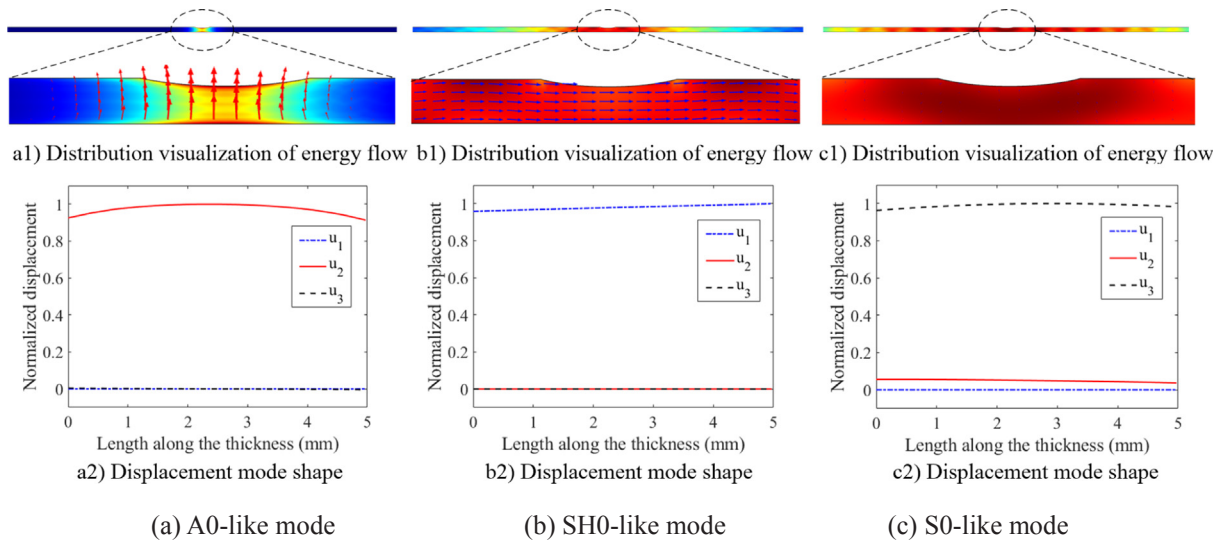
a1) Distribution visualization of energy flow   b1) Distribution visualization of energy flow   c1) Distribution visualization of energy flow

a2) Displacement mode shape   b2) Displacement mode shape   c2) Displacement mode shape

(a) A0-like mode   (b) SH0-like mode   (c) S0-like mode

Fig. 11. Modal shapes of three modes of weld-guided waves at 120 kHz for 18 mm width concave cross section.

when other geometric parameters remain unchanged, the larger the width of the weld zone, the more obvious the energy trapping effect of the weld zone will be. The modal characteristics of A0-like mode in the parametric model with a width of 18 mm are very similar to those in the actual FSW model in Section 3.

4.3. Parametric analysis of the modulus ratio-change weld-guided waves

The purpose of this parametric analysis is to investigate the effects of changing the modulus of WZ and BMZ on the propagation characteristics even without the structural feature variation (i.e. h_1 is zero). As stated in Section 2.1, this investigation has practical significance, since the geometric discontinuity of a weld cross section can be eliminated by using a non-shoulder-plunge welding tool. In this case, there is only a difference in the Young's modulus. When the values listed in Table 3 are put into the parametric models applied by SAFE method at 120 kHz, the existences of three A0-like, SH0-like and S0-like modes are listed in Table 4.

The process of justifying the existence of three modes can be described as follows. (1) For a specific ratio, looking for eigenvalues of wave number for a chosen frequency values is repeated in their small adjacent range to reveal all of the possible modes by SAFE method. (2) For each found eigenvalue, the corresponding energy flow distribution and vibration modes at three direction obtained by SAFE method, are jointly used to determine the existence of weld-guided waves modes in the weld zone. It can be found that no weld-guided waves are observed when $r < 1$, while some modes of weld-guided waves can be found when $r > 1$. For examples, three A0-like, SH0-like and S0-like modes

Table 4
The existences of the three modes at 120 kHz, determined by SAFE, when changing the modulus ratio r.

r		A0-like mode	SH0-like mode	S0-like mode
$r < 1$	$E_{BMZ} : E_{WELD} = 1{:}1.3$	no	no	no
	$E_{BMZ} : E_{WELD} = 1{:}1.2$	no	no	no
	$E_{BMZ} : E_{WELD} = 1{:}1.1$	no	no	no
	$E_{BMZ} : E_{WELD} = 1{:}1.07$	no	no	no
$r > 1$	$E_{BMZ} : E_{WELD} = 1{:}0.9$	yes	yes	yes
	$E_{BMZ} : E_{WELD} = 1{:}0.8$	no	yes	yes
	$E_{BMZ} : E_{WELD} = 1{:}0.7$	no	no	yes
	$E_{BMZ} : E_{WELD} = 1{:}0.6$	no	no	yes
	$E_{BMZ} : E_{WELD} = 1{:}0.5$	no	no	no

Note: the value of r shaded by yellow is the same as that of the FSW model in Section 3.

can be found in the case of $E_{BMZ} : E_{WELD} = 1{:}0.9$; S0-like mode exist in the cases of four ratio except of $r = E_{BMZ} : E_{WELD} = 1{:}0.5$.

In the case $E_{BMZ} : E_{WELD} = 1{:}0.9$, the three modes of weld-guided waves at 120 kHz are shown in Fig. 12, in terms of the energy flow distribution and the displacement mode shape. It can be seen that the modal characteristics of A0-like mode in the modulus-changing FSW model is still similar to those in the real FSW model and the geometric FSW model, while SH0-like mode and S0-like mode show different propagation characteristics than those in the previous two FSW models. From their distributions of energy flows of Figs. 12 and 11, it can be shown that most energy of SH0-like mode and S0-like mode at 120 kHz can be concentrated in the welded zone, which means the leakage effects of SH0-like and S0-like mode are not much significant as those in the geometric discontinuity FSW model. Meanwhile, it can be observed that the curve shapes of normalized energy flow along the width direction of the weld cross-section are much smoother than those in Section 4.2, especially for S0-like mode. The reason for this smooth shape is due to the boundary geometric continuity of the weld cross section.

According to the previous results of Section 4, it can be seen that three fundamental modes (A0-like, S0-like and SH0-like) of weld-guided waves at 120 kHz will be not observed in the weld zone of a FSW joint when the modulus of the weld zone is greater than that of the base material zone. When the modulus ratio of the weld zone over the base material zone is greater than 1, some similar modes of weld-guided waves will be found and their energy can be concentrated in the weld zone and its around region. Compared with the results of Section 3 and Section 4, it can be also found that the modulus ratio-change weld-guided waves show more obvious energy trapping effect in and near to the weld zone than the width-change weld-guided wave. According to numerical results of two parametric studies, it can also be implied that the existence of A0-like weld-guided waves in a given real FSW model is the result of the coupling interaction of feature guided waves with structural geometry feature and modulus discontinuity. The investigation of natural reasons should be further performed systematically by different combination of cross-sectional geometric shape and material properties.

5. Experimental validation

5.1. The experimental setup

In order to validate the energy concentration effect of the weld-guided mode, the experiment is designed and carried out on a 2119
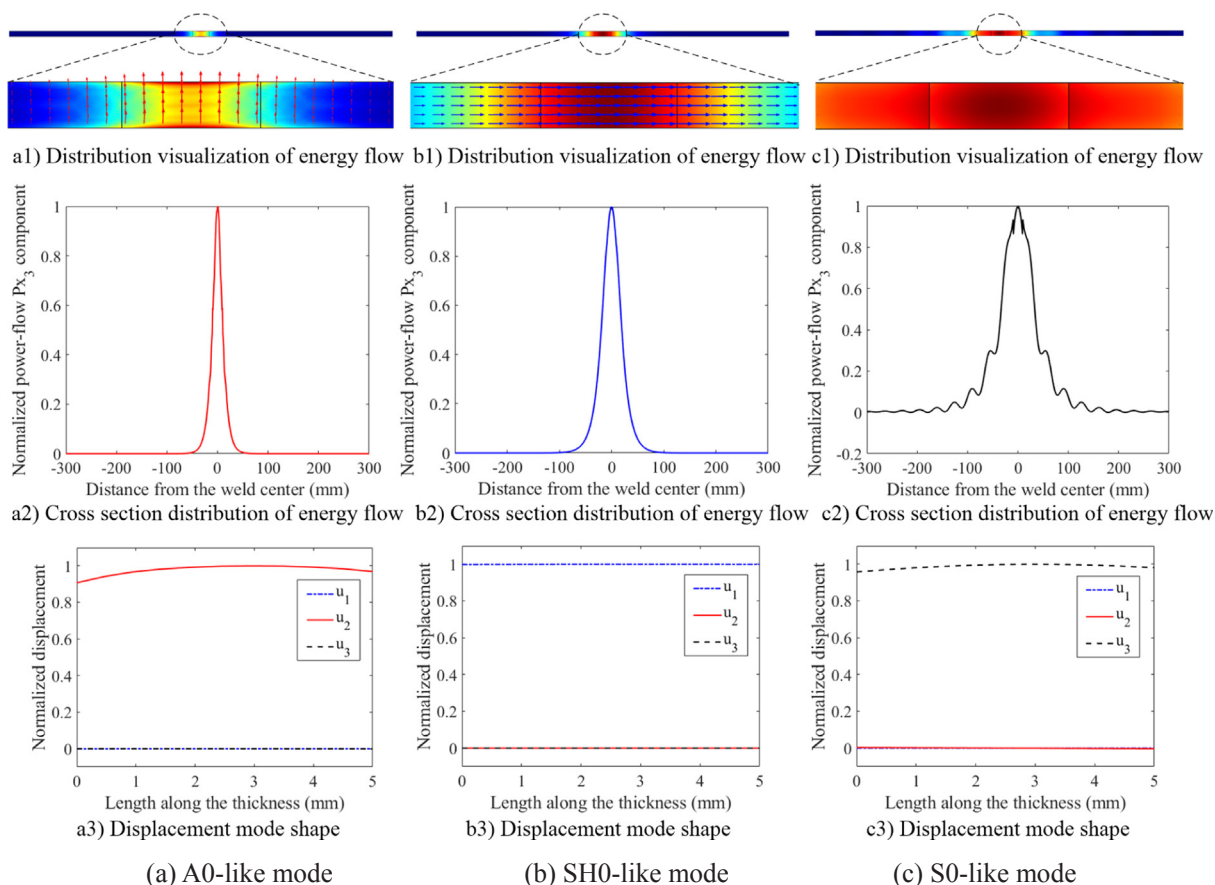
a1) Distribution visualization of energy flow   b1) Distribution visualization of energy flow   c1) Distribution visualization of energy flow

a2) Cross section distribution of energy flow   b2) Cross section distribution of energy flow   c2) Cross section distribution of energy flow

a3) Displacement mode shape   b3) Displacement mode shape   c3) Displacement mode shape

(a) A0-like mode   (b) SH0-like mode   (c) S0-like mode

Fig. 12. Modal shapes of three WGWs at 120 kHz in an 18-mm-width weld with uniform cross section (r = 1:0.9).
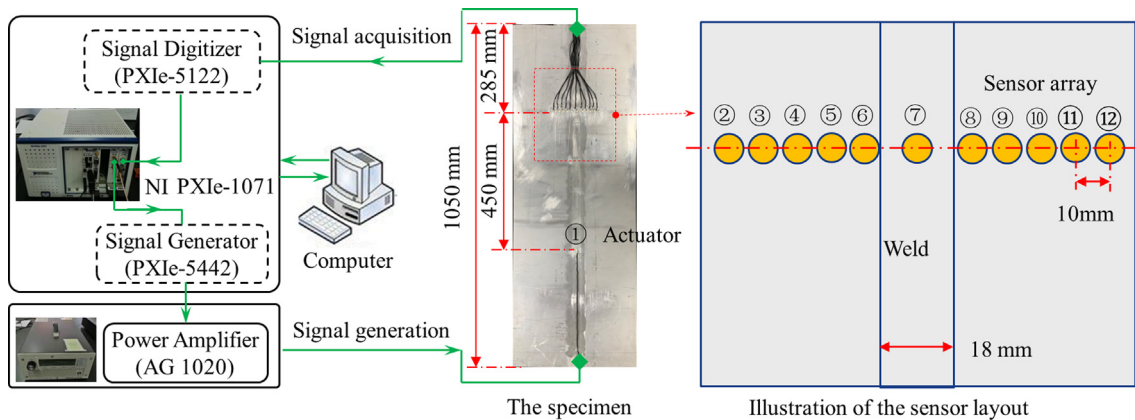

Fig. 13. Photograph of experimental setup and sensor layout of the specimen II.

aluminum alloy FSW plate (type II listed in Table 1). The transducers are PZT-5A circular wafers (8 mm diameter and 0.44 mm thickness). The polarization of PZT is along the thickness direction. One PZT transducer marked by ① was bonded at the weld center as an actuator, and driven by a function generator (NI PXIe-5442) producing a 5-cycle Hanning windowed toneburst that is then amplified by the power amplifier AG1020. The sensor signals were acquired by NI PXIe-5122 signal digitizer with a sampling rate 20 MHz. The experimental setup is shown in Fig. 13.

The sensor layout scheme of the specimen was illustrated in Fig. 13. A linear array with eleven PZT sensors was symmetrically attached to two sides of the specimen II. The middle sensor in the array was located at the weld center line, marked by ⑦ in the specimen II, respectively. The distance between the actuator and the middle sensor was 450 mm.

The distance between two adjacent sensors was 10 mm, except the middle three sensors.

5.2. The experimental results and discussion

The five-cycle Hanning windowed toneburst signal at different frequencies from 100 kHz to 500 kHz by a 10 kHz step was input to the actuator to excite the FSW joint of the specimen II. The arrayed sensors received the time-domain signals. The enveloped signals at 120 kHz were listed in Fig. 14.

As shown in Fig. 15, the measured signal acquired by the sensor ⑦ in the weld zone was used to calculate the group velocity (short for C_g) of the A0-like mode at 120 kHz. The group velocity of the A0-like wave packet of the measured signals at a chosen frequency can be calculated
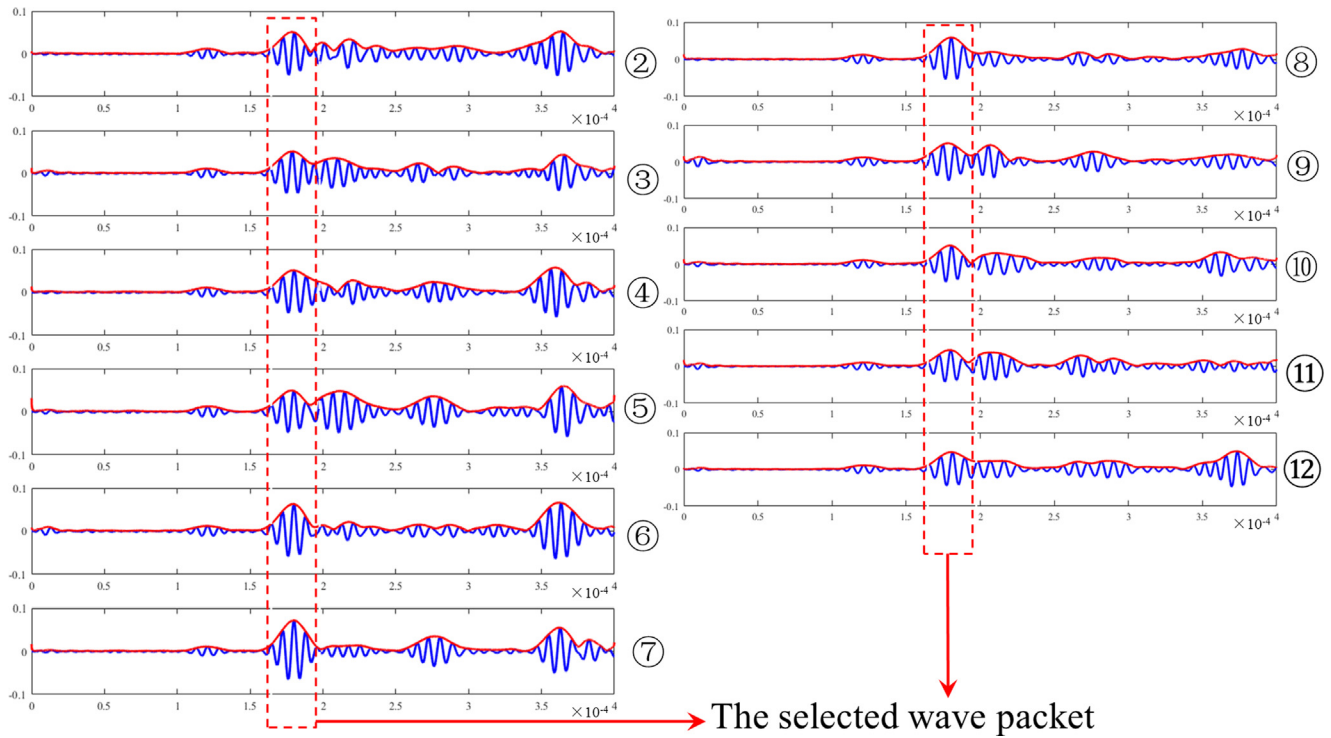
Y. Wang, et al.

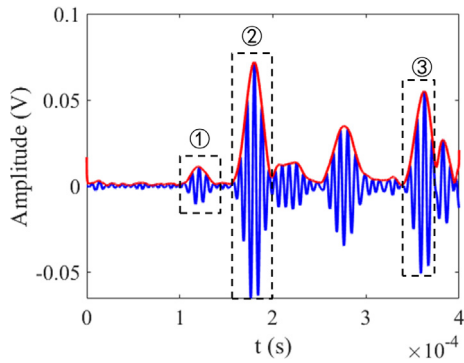Fig. 14. Time-domain enveloped signals at 120 kHz acquired by the eleven sensors.

Fig. 15. Time-domain enveloped signals at 120 kHz acquired by the sensor ⑦ in the weld zone.

Fig. 16. Measured normalized amplitude of A0 mode waves along the weld width direction.

by the shift of the Hilbert envelope of wave packets. The wave packet marked by ① is a S0 mode wave. The wave packet ② is used to calculate the C_g value as 2830.2 m/s. However, the predicted group velocity of the A0-like mode at 120 kHz by SAFE in Section 3.4 is about 3129 m/s. The relative error between the two C_g values is about 9.5%.So the wave packet ② is identified as A0-like mode wave. While the wave packet ③ is the signals reflected by the upper boundary, which is used to verify the correctness of the calculated C_g value. The propagation distance of the wave packet ③ reflected by the upper boundary was determined as 966.7 mm by multiplying the time of flight with the calculated C_g. The real distance should be 1020 mm (450 mm + 2*285 mm) as shown in Fig. 13.

The normalized maximum amplitudes of the selected wave packets marked by a rectangular dotted frame in Fig. 14 at given frequencies from 100 kHz to 170 kHz by a 10 kHz step are compared to illustrate the energy concentration phenomenon shown in Fig. 16. It can be clearly seen that the amplitude of A0-like wave packet acquired by the middle sensor in the weld zone is higher than those by other sensors away from the weld zone. The energy trapping effect means that the energy of A0-like weld-guided waves is concentrated in and around the
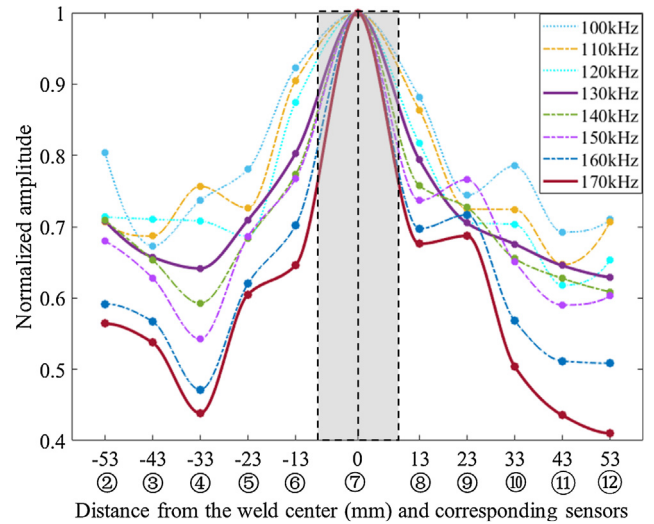
weld region of the FSW plate. It should be noted that the measured energy distribution of the interesting A0-like weld-guided wave mode is not fit well with the result shown in Fig. 8(c) as the distance deviated from the weld center. This phenomenon of relative high amplitude in the BMZ is caused by the A0 mode simultaneously excited in the adjacent plate as well as the reflection signals from the side boundary.

According to the simulation of SAFE model of a given FSW plate, the A0-like weld-guided waves will not leak energy into the plate when propagating, which is physically the perfect energy trapping effect. However, it is very difficult to obtain this ideal result in the experiment by bonding the PZT sensors on the surface of FSW plate. The ideal excitation situation is that only the A0-like mode propagating along the weld is excited, while the accompanying excitation of A0 and S0 modes is restrained effectively. Therefore, the farther the propagation distance

is, the clearer the intrinsic observation of A0-like weld-guided waves will be. Meanwhile, the energy trapping effect can be validated in better ways by signal acquisition techniques such as fiber sensor and laser sensor, and signal processing techniques. Therefore, the future work should focus on the modal separation by advanced signal processing techniques.

6. Conclusion

The propagation characteristics of ultrasonic weld-guided waves in the same-material FSW joint are theoretically and numerically investigated to illustrate that different weld-guided wave can propagate in the weld zone of FSW joint. The weld zone of FSW joint is featured with a thinning cross section, complex mircostructure and mechanical properties due to complex friction stir welding process. Some FSW joint specimens cut from a 2219 aluminum alloy FSW plate are used to perform metallographic analysis and mechanical tests including microhardness, modulus and density. Based on these geometries and material properties, a SAFE model of the FSW joint is developed. The experiments are carried out to validate the existence of A0-like weld-guided mode due to energy trapping effect.

To systematically investigate the possible effects of geometrical and mechanical factors on the propagation behaviors of weld-guided waves, a respective parametric analysis of two single parameters (the width of concave cross-sectional weld zone and the modulus values of different zones) is conducted. It is also found that the geometric discontinuity plays a dominant role in forming weld-guided waves in the given FSW model. When the weld width is changed while the moduli of the welded zone and base metal zone are maintained the same, three weld-guided waves (A0-like mode, SH0-like mode and S0-like mode) always exist. When the cross section is geometrically continuous (i.e. the shoulder plunge depth is zero), it is observed that the weld-guided waves at 120 kHz only exist if the modulus value of the welded zone is lower than that of the base metal zone. Comparing with width-change weld-guided waves, the modulus ratio-change weld-guided waves shows less obvious energy leakage.

Although this study has focused on both concave weld geometry and modulus ratio of the welded zone to the base metal zone, it is clear that the coupling mechanism of these two features for forming the guiding effect still need to be further investigated. Meanwhile, the advanced signal processing techniques should be developed to separate the weld-guided waves of interesting mode from the time-domain signals. The potential of using weld-guided waves for inspection the flaws of FSW joint will be further studied.

Acknowledgments

References

[1] B.T. Gibson, D.H. Lammlein, T.J. Prater, W.R. Longhurst, C.D. Cox, M.C. Ballun, K.J. Dharmaraj, Friction stir welding: process, automation, and control, J. Manuf. Processes 16 (2014) 56–73.

[2] M. Su, C.F. Xu, Aerospace industry standards comparative analysis of friction stir welding and fusion welding, Aerosp. Standardizat. 1 (2010) 15–19.

[3] R.S. Mishra, Z.Y. Ma, Friction stir welding and processing, Mater. Sci. Eng. R50 (2010) 1–78.

[4] C.Q. Huang, H. Li, J.X. Li, C.G. Luo, Y.B. Ni, Residual stress measurement on propellant tank of 2219 aluminum alloy and study on its weak spot, J. Mech. Sci. Technol. 31 (2017) 2213–2220.

[5] T. Saravanan, B.B. Lahiri, K. Arunmuthu, S. Bagavathiappan, A.S. Sekhar, Non-destructive evaluation of FSW joints by X-ray radiography and infrared thermograph, Procedia Eng. 86 (2014) 469–475.

[6] S.P. Liu, F.F. Liu, L.G. Li, E.M. Guo, R.C. Wang, Investigation of ultrasonic method based on different incident angles for evaluation of friction stir wieding, Non-Destr. Test. 5 (2006) 225–228.

[7] L.S. Rosado, T.G. Santos, M. Piedade, P.M. Ramos, et al., Advanced technique for non-destructive testing of friction stir welding of metals, Measurement 43 (2010) 1021–1030.

[8] R.A. Smith, The potential for friction stir weld inspection using transient eddy currents, Insight – Non-Destruct. Testing Condit. Monitor. 47 (2005) 133–143.

[9] Z. Su, L. Ye, Y. Lu, Guided Lamb waves for identification of damage in composite structures: a review, J. Sound Vib. 295 (3) (2006) 753–780.

[10] C. Zhou, C.L. Zhang, Z.Q. Su, et al., Health monitoring of rail structures using guided waves and three-dimensional diagnostic imaging, Struct. Contr. Health Monitor. 24 (9) (2017) e1966.

[11] K.H. Liu, Z.J. Wu, Y.Q. Jiang, Y.S. Wang, K. Zhou, Y.P. Chen, Guided waves based diagnostic imaging of circumferential cracks in small-diameter pipe, Ultrasonics 65 (2016) 34–42.

[12] L. Qiu, S.F. Yuan, F.K. Chang, Q. Bao, H.F. Mei, On-line updating Gaussian mixture model for aircraft wing spar damage evaluation under time-varying boundary condition, Smart Mater. Struct. 23 (12) (2014) 125001.

[13] J. Yan, H. Jin, H. Sun, X. Qing, Active monitoring of fatigue crack in the weld zone of bogie frames using ultrasonic guided waves, Sensors 19 (2019) 3372.

[14] X. Qing, W. Li, Y. Wang, H. Sun, Implementation of piezoelectric transducer based structural health monitoring for aircraft application, Sensors 19 (3) (2019) 545.

[15] J.P. Sargent, Corrosion detection in welds and heat-affected zones using ultrasonic Lamb waves, Insight-Non-Destruct. Test. Condit. Monitor. 48 (2006) 160–167.

[16] X. Yu, Z. Fan, M. Castaings, C. Biateau, Feature guided wave inspection of bond line defects between a stiffener and a composite plate, NDT E Int. 89 (2017) 44–55.

[17] P. Rajagopal, R.K. Pattanayak, Ultrasonic guided waves in elliptical annular cylinders, J. Acoust. Soc. Am. 138 (2015) 336–341.

[18] Zheng Fan, Mike J.S. Lowe, Elastic waves guided by a welded joint in a plate, Proc. R. Soc. A 465 (2107) (2009) 2053–2068, https://doi.org/10.1098/rspa.2009.0010.

[19] X. Yu, M. Ratassepp, P. Rajagopal, Z. Fan, Anisotropic effects on ultrasonic guided waves propagation in composite bends, Ultrasonics 72 (2016) 95–105.

[20] X. Yu, P. Zuo, J. Xiao, Z. Fan, Detection of damage in welded joints using high order feature guided ultrasonic waves, Mech. Syst. Sig. Process. 126 (2019) 176–192.

[21] Z. Fan, M.J.S. Lowe, Interaction of weld-guided waves with defects, NDT and E Int. 47 (2012) 124–133.

[22] X. Yu, P. Manogharan, Z. Fan, P. Rajagopal, Shear horizontal feature guided ultrasonic waves in plate structures with 90 transverse bends, Ultrasonics 65 (2016) 370–379.

[23] M. Castaings, M. Lowe, Finite element model for waves guided along solid systems of arbitrary section coupled to infinite solid media, J. Acoust. Soc. Am. 123 (2) (2008) 696.

[24] M.V. Predoi, M. Castaings, B. Hosten, C. Bacon, Wave propagation along transversely periodic structures, J. Acoust. Soc. Am. 121 (4) (2007) 1935.

[25] M. Castaings, B. Hosten, Ultrasonic guided waves for health monitoring of high-pressure composite tanks, NDT and E Int. 41 (8) (2008) 648–655.

[26] X. Yu, M. Ratassepp, Z. Fan, Damage detection in quasi-isotropic composite bends using ultrasonic feature guided waves, Compos. Sci. Technol. 141 (2017) 120–129.

[27] P. Ray, X. Yu, Z. Fan, B. Srinivasan, P. Rajagopal, Fiber bragg grating based detection of part-thickness cracks in bent composite laminates using feature-guided waves, Smart Mater. Struct. 28 (8) (2019) 085026.

[28] M.A. Fakih, S. Mustapha, J. Tarraf, G. Ayoub, R. Hamade, Detection and assessment of flaws in FSW joints using ultrasonic guided waves: experimental and finite element analysis, Mech. Syst. Sig. Process. 101 (2018) 516–534.

[29] J. Tarraf, S. Mustapha, M.A. Fakih, M. Harb, H.J. Wang, Application of ultrasonic waves towards the inspection of similar and dissimilar FSW joints, J. Mater. Process. Technol. 255 (2018) 570–583.

[30] M.A. Fakih, S. Mustapha, M.S. Harb. The interaction of the fundamental symmetric and antisymmetric Lamb wave modes with material discontinuity - a 3D finite element analysis. 7th Asia-Pacific Workshop for Structural Health Monitoring (APWSHM). Hong Kong SAR, China2018.

[31] B. Wu, C.Y. Cui, Y.C. Zhang, C.F. He, Journal of basic science and engineering, Propagat. Characterist. Influenc. Fact. Lamb Waves Butt Welds 4 (2014) 818–829.

[32] M.A. Fakih, J. Tarraf, S. Mustapha, M.S. Harb, H. Wang, G. Ayoub, R. Hamade, Characterization of Lamb waves propagation behavior in friction stir welded joints of dissimilar materials, Proceedings of the 11th International Workshop on Structural Health Monitoring (2017) 55–62.

[33] N. Juluri, M. Lowe, P. Cawley, The guiding of ultrasound by a welded joint in a plate, AIP Conf. Proc. (2007:) 894.

[34] H.R. Doude, J.A. Schneider, A.C. Nunes, Influence of the tool shoulder contact conditions on the material flow during friction stir welding, Metallurgic. Mater. Trans. A 45 (10) (2014) 4411–4422.

[35] G. Cam, S. Mistikoglu, Recent developments in friction stir welding of Al-alloys, J. Mater. Eng. Perform. 23 (2014) 1936–1953.

[36] M. Kumar, S.V. Kailas, R.G. Narayanan, Influence of external weld flash on the in-plane plane-strain formability of friction stir welded sheets, J. Strain Anal. Eng. Des. 48 (6) (2013) 76–385.

[37] H.J. Zhang, M. Wang, Z. Zhu, et al., Improving the structure-property of aluminum alloy friction stir weld by using a non-shoulder-plunge welding tool, Int. J. Adv. Manuf. Technol. 87 (2016) 1095–1104.

[38] G. Liu, L.E. Murr, C.S. Niou, et al., Microstructural aspect s of the friction-stir welding of 6061–T6 aluminum, Scr. Mater. 37 (3) (1997) 355–361.

[39] W.F. Xu, J.H. Liu, G.H. Luan, C.L. Dong, Temperature evolution, microstructure and mechanical properties of friction stir welded thick 2219-O aluminum alloy joints, Mater. Des. 30 (2009) 1886–1893.

[40] B.A. Auld, R.E. Green, Acoustic fields and waves in solids two volumes, Phys. Today 27 (10) (1974) 63–64.